NASA Technical Memorandum 105316

Thermomechanical Deformation Behavior of a Dynamic Strain Aging Alloy, Hastelloy X

Michael G. Castelli
Sverdrup Technology, Inc.
Lewis Research Center Group
Brook Park, Ohio

Robert V. Miner
National Aeronautics and Space Administration
Lewis Research Center
Cleveland, Ohio

and

David N. Robinson
University of Akron
Akron, Ohio

April 1992

NASA

THERMOMECHANICAL DEFORMATION BEHAVIOR OF A DYNAMIC STRAIN AGING ALLOY, HASTELLOY X

Michael G. Castelli
Sverdrup Technology, Inc.
Lewis Research Center Group
Brook Park, Ohio 44142

Robert V. Miner
National Aeronautics and Space Administration
Lewis Research Center
Cleveland, Ohio 44135

and

David N. Robinson
University of Akron
Akron, Ohio 44325

E-6899

ABSTRACT

An experimental study was performed to identify the effects of dynamic strain aging (solute drag) and metallurgical instabilities under thermomechanical loading conditions. The study involved a series of closely controlled thermomechanical deformation tests on the solid-solution-strengthened nickel-base superalloy, Hastelloy X. This alloy exhibits a strong isothermal strain aging peak at approximately 600 °C promoted by the combined effects of solute drag and precipitation hardening. Macroscopic thermomechanical hardening trends are correlated with microstructural characteristics through the use of transmission electron microscopy. These observations are also compared and contrasted with isothermal conditions. Thermomechanical behavior unique to the isothermal database is identified and discussed. The microstructural characteristics were shown to be dominated by effects associated with the highest temperature of the thermomechanical cycle. Results indicate that the deformation behavior of Hastelloy X is thermomechanically path dependent. In addition, guidance is given pertaining to deformation modeling in the context of a macroscopic unified viscoplastic constitutive theory. An internal state variable is formulated to qualitatively reflect the isotropic hardening trends identified in the TMD experiments.

INTRODUCTION

Structural components used in high temperature applications will often experience inelastic deformation resulting from mechanical loading, thermal transient cycles, and thermal gradients. Such forms of combined thermal and mechanical loading can potentially promote material behavior which is different from that exhibited under idealized isothermal conditions. The potential for these differences is greatly increased if the material is inclined to experience various temperature-stress-time dependent microstructural changes, such as those promoted by thermal, static, and dynamic aging mechanisms.

One such mechanism of key interest in this investigation is termed dynamic strain aging (ref. 1). Dynamic strain aging (solute drag) effects are exhibited by many alloys of common use, including austenitic stainless steels and many Co- and Ni-base alloys. At temperatures where this phenomenon is

present, the material will experience a relative increase in flow stress and work hardening rate, and various forms of inhomogeneous deformation. For the Ni-base superalloy, Hastelloy X,* dynamic strain aging has been noted to contribute to complex isothermal hardening trends (ref. 2), raising obvious questions about its influence under more prototypical thermomechanical conditions.

In addition, many materials prone to dynamic strain aging effects are also subject to various forms of metallurgical instabilities. Typically, such instabilities result in the precipitation of a new micro-structural phase (refs. 3 to 7), the introduction of which can promote deformation behavior different from that observed prior to the precipitation. Microstructural changes of this nature often lead to an increase in dislocation density and dislocation pinning, thereby enhancing the strain hardening behavior of the material. Consequently, at any given isothermal loading condition, the combined effects of precipitation hardening and dynamic strain aging can produce a highly complex macroscopic hardening behavior. This behavior is, in turn, potentially further complicated through the introduction of thermomechanical conditions.

This work examines the hardening response of a dynamic strain aging alloy under thermo-mechanical loading. A series of closely controlled thermomechanical deformation (TMD) tests were conducted on Hastelloy X. Hastelloy X was chosen as a model material because of its common use in high temperature power generation applications. Also, the strong dynamic strain aging effects in Hastelloy X are experienced at temperatures of most common use. Isothermal and thermomechanical material response are examined and compared on the basis of deformation trends and microstructural observations. The micro-structural mechanisms responsible for the cyclic hardening will be briefly discussed; a more detailed examination of the relative contributions between solute drag and precipitation hardening in Hastelloy X is published elsewhere (ref. 8). Observations made from both the macroscopic and microscopic arenas are linked to help explain unique phenomenological trends experienced under thermomechanical conditions.

Upon gaining an understanding of the microstructural physics and their influence on TMD behavior, an established macroscopic unified thermoviscoplastic constitutive theory (refs. 9 and 10) is introduced and extended to qualitatively reflect the observed trends. This extension involves the introduction of an internal state variable to track the phenomenological effects of precipitation hardening and dynamic strain aging. The proposed framework is established with emphasis placed on modeling the isotropic hardening behavior.

MATERIAL

Hastelloy X is a nickel-base solid-solution-strengthened alloy with good corrosion and oxidation resistance at temperatures up to 1100 °C. Its composition is nominally 22Cr, 18.5Fe, 9Mo, 0.6W, 1.5Co, and 0.1C, all in weight percent, with the balance being Ni. Typically supplied in a solution treated state, the as received microstructure consists of an FCC solid-solution matrix with a sparse distribution of Mo-rich M_6C carbides. The material heat specific to this investigation was produced in accordance with Aerospace Material Specification 5754H. Mechanical test specimens were machined from solution treated 19 mm diameter bar stock.

*Hastelloy is a trademark of Stoody Deloro Stellite, Inc., Industry, CA.

HARDENING MECHANISMS IN HASTELLOY X

Dynamic Strain Aging

The phenomenon of dynamic strain aging (ref. 1) occurs in solid solutions where solute atoms are particularly free to diffuse (either interstitial or substitutional solutes may contribute at appropriate temperatures) through the parent lattice. It is energetically preferable for these solute atoms to occupy sites in the vicinity of dislocations where they form solute (Cottrell) atmospheres (ref. 11) around the dislocations. This temporary solute atmosphere impedes subsequent dislocation movement and thus causes strengthening, as revealed by a relative increase in flow stress. With increasing strain rate, the dislocations begin to move too fast to allow the atmosphere to diffuse with them and as a result, the solute atmosphere becomes progressively more dilute. The overall effect reduces the solute drag force with increasing dislocation velocity, giving rise to an inverse strain rate/flow stress sensitivity. Dynamic strain aging is also associated with several forms of inhomogeneous deformations, termed Portevin-le Chatelier effects (ref. 12). Mechanisms promoting such behavior include the sudden creation and/or mobilization of formerly pinned dislocations. These fast moving dislocations (free of solute atmospheres) give rise to sudden stress drops, more commonly referred to as jerky flow or serrated yielding.

Cyclic loading at temperatures where dynamic strain aging mechanisms are active results in marked material hardening. This behavior is evidenced by an increased hardening rate and hardening range. For any given dynamic strain aging alloy, an intermediate temperature range exists where the hardening rate and cyclic saturation strength is maximized. This maxima is interpreted as a manifestation of dynamic strain aging, and is typically referred to as the dynamic strain aging peak. At temperatures below the dynamic strain aging range, solute diffusion will not take place. At temperatures above, normal thermal recovery processes (e.g., dislocation climb) will dominate.

Precipitation Hardening

In general, many alloys experience various forms of microstructural instabilities leading to the precipitation of a wide variety of new phases. However, to maintain applicability to the work at hand, this brief generalized discussion will be limited to the precipitation of the $M_{23}C_6$ carbide phase in Hastelloy X. In the solution treated condition, Hastelloy X is found to contain only the solid solution matrix and a sparse distribution of Mo-rich M_6C carbides. The M_6C phase is unstable in a Cr-rich environment and consequently, thermal aging at intermediate temperatures results in the precipitation of a Cr-rich $M_{23}C_6$ carbide phase (refs. 13 and 14). In addition to the effects associated with a static thermal age, experiments (ref. 7) have suggested that a significant amount of deformation-assisted $M_{23}C_6$ precipitation occurs as a result of the dislocations' powerful affect on lowering the nucleation barrier (ref. 15) and becoming preferred carbide nucleation sites.

In its initial state, the $M_{23}C_6$ phase is relatively small (10 to 100 nm (ref. 8)) and highly effective at dislocation blocking and pinning; hence notable material hardening is experienced. Under isothermal loading conditions, the peak effectiveness of the precipitation hardening in Hastelloy X occurs in the temperature range of about 500 to 650 °C, thus partially overlapping the 200 to 700 °C range of dynamic strain aging. This precipitation strain aging peak is also typically associated with a ductility minimum. Aging at temperatures above the precipitation strain aging peak, the $M_{23}C_6$ carbide undergoes considerable growth. In this enlarged, overaged state, the phase appears to be considerably less effective as a hardening mechanism.

TEST METHODS

Cyclic Isothermal Deformation

Isothermal data taken from a previous experimental study conducted by Ellis et al. (ref. 2) is presented to enable comparisons with the TMD data generated in this study. All isothermal deformation tests were performed in air under strain control with constant cyclic axial-strain amplitudes of ± 0.003. A constant strain rate of 0.0001 s^{-1} was used with a triangular command waveform. Strains were controlled over a 25.4 mm parallel gage section with a high temperature water cooled axial extensometer. Specimen heating was accomplished through the use of direct induction coils. Isothermal conditions from room to 1000 °C were investigated. Temperature gradients were maintained in accordance with the ASTM recommended standard for constant-amplitude low-cycle fatigue (E606). Unless otherwise noted, the isothermal tests were terminated at 10^4 cycles or evidence of the first macro-crack, whichever occurred first.

Cyclic Thermomechanical Deformation

As the main interest of this investigation involved characterizing the hardening (stress change) behavior of Hastelloy X under TMD conditions, it was necessary to conduct the experiments under strain control. In addition, a fixed mechanical strain range was desired to facilitate comparisons with existing isothermal data. Axial mechanical strain controlled TMD experiments are difficult to perform accurately because the total strain measurement (controlling variable) is directly influenced by a change in temperature (thermal expansion strains). Several advances were made in the area of thermomechanical testing techniques and procedures, discussed elsewhere (ref. 16), which enabled the experiments to be conducted under closely controlled conditions and thus made the isothermal comparisons possible.

The thermomechanical test matrix is shown in table I. In-phase and out-of-phase conditions involving temperatures from 200 to 1000 °C were conducted with temperature ranges of 200 °C. Two relatively large temperature ranges were examined to establish the effects of cycling completely through the strain aging peak regime. Phasing is defined by the relationship between the mechanical strain waveform and the temperature waveform. Thus, a test is defined to be "in-phase" when these two waveforms are coincidental, and "out-of-phase" when the two waveforms are phased with a time shift equal to one-half the cycle period. The mechanical strain (ϵ^m) is defined as the difference between the total (e^t) and thermal (ϵ^{th}) strains, i.e.,

$$\epsilon^m = e^t - \epsilon^{th}.$$

All TMD tests were conducted in air with cyclic mechanical strain amplitudes of ± 0.003 and a constant temperature rate of 100 °C/min, independent of temperature range. Given the fixed mechanical strain range and temperature rate, the mechanical strain rate was calculated based on temperature range. Note that the strain rate for the thermomechanical tests (with $\Delta T = 200$ °C the mechanical strain rate is 5.0×10^{-5}/s) was slightly less than that used for the isothermal data taken from (ref. 2) (1.0×10^{-4}/s). The effects of strain rate from 1.0×10^{-3}/s to 3.0×10^{-5}/s were examined for this material (unpublished data by Allen et al. at NASA Lewis) and found to have a negligible effect on the magnitude of isotropic hardening. Therefore, the factor-of-two difference between the thermomechanical and isothermal data was assumed to have a negligible effect on the isotropic hardening behavior.

The test specimens were heated with direct induction heating. Specimen cooling was accomplished through the use of water cooled grips; no forced air was used. A triangular waveform was used for both the temperature and strain. The strains were controlled over a 12.7 mm parallel gage section with a high

temperature water-cooled axial extensometer. A thin-walled tube specimen design was developed and used for this study, as it was found to perform superior to the solid cylindrical specimen under TMD conditions (ref. 16).

Microstructural Examination

Specimens for transmission electron microscopy (TEM) were obtained from the wall in the gage section of the tubular test specimens by electrodischarge machining. The specimens were prepared by fine grinding and electropolishing to perforation. Electropolishing was accomplished in a solution of 10 percent Perchloric acid, 45 percent Butanol and 45 percent Methanol at 0 °C and 30 V.

RESULTS AND DISCUSSION

Cyclic Isothermal Deformation

Shown in figure 1 are plots of stress amplitude ($\frac{1}{2}\Delta\sigma$) verses cycle, revealing the isothermal cyclic hardening behavior of Hastelloy X. Because the tests are conducted under strain control, the stress amplitudes are free to increase (harden) or decrease (soften) as material response dictates. The isothermal data did not reveal a noteworthy mean stress during fully-reversed strain cycling; thus the stress amplitude value shown is representative of that which occurred in both tension and compression. Figure 1 displays hardening curves over three generalized temperature domains approximately bounded by room temperature to 200, 200 to 650, and 650 to 1000 °C, subsequently referred to as "low," "middle," and "high," respectively.

In the low temperature domain, the isothermal cyclic response of Hastelloy X is essentially neutral with respect to hardening. Stress amplitude increases of only 10 to 15 percent (with respect to first cycle values) were realized before a state of cyclic saturation was reached.

This trend quickly changed as temperatures increase into the middle temperature domain, figure 1(b), encompassing the strain aging peak. Tests performed at 316 and 427 °C exhibited an increase in stress amplitude of 60 and 66 percent, respectively. Hardening continues to increase through the middle temperature domain until a maximums are realized at 500 to 650 °C. Here, increases greater than 85 percent can be experienced. Serrated yielding was noted in a surprisingly small percentage of the specimens tested in this temperature domain. However, other evidences indicating dynamic strain aging, such as an inverse strain rate/flow stress sensitivity, were consistently and clearly identified. Further, the dynamic strain aging range is felt to begin at temperatures as low as 200 °C, where marked hardening and increased dislocation densities were observed (ref. 8).

The transition from the middle to the high temperature domain is established by surpassing the strain aging peak temperature. In this temperature domain figure 1(c), cyclic hardening drops significantly with a relatively small increase in temperature. At 704 °C, the percent increase in stress amplitude drops from over 85 at 650 °C to 44. The decrease continues until cyclic softening occurs during tests performed at 870 °C and above.

The phenomenological hardening effects of dynamic strain aging on Hastelloy X are best summarized in figure 2. Stress amplitudes are plotted at intermittent cycles over the full working temperature range. The test conducted at 427 °C was terminated prematurely at approximately

5000 cycles because of a heater problem. This figure clearly reveals that the strain aging is maximized in the general temperature range of 400 to 600 °C.

Isothermal Microstructures

TEM was used to identify the physical characteristics associated with the various hardening behaviors exhibited in the isothermal tests. Examination revealed general microstructural features uniquely associated with the three temperature domains (low-middle-high) discussed above. Dislocation substructures representative of these features were taken from specimens tested at 93, 650, 538, and 871 °C and are shown in figure 3.

Micrographs taken from specimens tested in the low temperature domain, such as that shown in figure 3(a), reveal a relatively low dislocation density. The imposed temperature and mechanical loading conditions do not appear to have affected the stability of the M_6C carbide phase (present in the as-received condition), as no new phases can be identified. Slip is inhomogeneous and the dislocations are found primarily concentrated in a few planar slip bands. These general features support the observations of relatively low cyclic hardening in the low temperature domain.

In the specimens examined from the middle temperature domain, there are two distinct physical changes observed, (1) a dramatically increased dislocation density and (2) the precipitation of the $M_{23}C_6$ phase. The first visually detectable change in the microstructure is the relative increase in dislocation density, as revealed in figure 3(b). Dislocation densities (at 10^4 cycles or failure, whichever occurred first) steadily increase from the values found at 200 °C to those observed at temperatures of 500 to 600 °C, representing the maximum values (quantitative results are addressed elsewhere (ref. 8)). This increased dislocation production can result from either hardening mechanism. Both, (1) dynamic strain aging (solute drag) and, (2) $M_{23}C_6$ precipitation will hinder the movement of existing dislocations and enhance the production of additional dislocations to accommodate the applied strain.

Given that dynamic strain aging effects have been identified over the temperature range of 200 to 700 °C, it is important to note at what point precipitation of the $M_{23}C_6$ phase begins; this information is critical to the understanding of the thermomechanical deformation. TEM observations and mathematical modeling of the $M_{23}C_6$ precipitation kinetics (ref. 8) both agree and show with certainty that this secondary carbide phase did not precipitate during the isothermal tests conducted below 500 °C. Therefore, the marked hardening experienced below this temperature, such as that observed at 316, 427, and 482 °C can be attributed to the effects of dynamic strain aging (fig. 2). At temperatures above 500 °C, $M_{23}C_6$ precipitation will occur (given sufficient time) and the hardening will be influenced by the combined effects of dynamic strain aging and precipitation hardening.

Examination of the 650 °C microstructure, shown in figure 3(c), reveals a slightly reduced dislocation density and a slightly larger $M_{23}C_6$ phase than those found in the 538 and 593 °C specimens. At this size ($\approx$60 nm in diam), the $M_{23}C_6$ phase is visible in a conventional bright-field image, pictured in figure 3(c) as the numerous dark circular objects. This phase is present but not visible in figure 3(b) because of the extremely small carbide size ($\approx$5 nm in diam). The increased size of the $M_{23}C_6$ carbide found at 650 °C suggests early stages of microstructural overaging.

Microstructures of specimens tested in the high temperature domain (T > 650 °C) begin to reveal features of thermally activated processes. The high temperature conditions promote dissolution of the original M_6C carbides, which become less numerous. The $M_{23}C_6$ carbides have undergone considerable physical growth and appear to have migrated to cell boundaries and twin boundaries. At the higher

temperatures of this domain, figure 3(d), large cells and subcells appear with low intracellular dislocation densities. The majority of dislocations are located at cell and twin boundaries, displaying well ordered arrangements. Cyclic tests at these relatively high temperatures typically results in a slight isotropic softening of the material.

Cyclic Thermomechanical Deformation

One of the main objectives of this study is to determine if the thermomechanical hardening trends of Hastelloy X are similar to those found under isothermal conditions. Although the TMD tests were conducted with the same mechanical strain range as the isothermal tests, direct data comparisons are still complicated by the respective temperature conditions. This is because a single TMD test involves a wide range of temperatures and an isothermal test, by definition, involves a single temperature. The approach taken for data comparisons in this study involves presenting the thermomechanical data along with "bounding" isothermal data, where bounding refers to the upper and lower test temperature. For ease of presentation, all stress amplitudes will be plotted according to their absolute values.

Displayed in figure 4 are results from TMD tests performed with a temperature range of 200 to 400 °C. The six curves represent data taken from four tests. The in-phase and out-of-phase TMD tests are each represented by two curves; one represents the peak tensile amplitudes and the other represents the peak compressive amplitudes. The two remaining curves are the bounding isothermal amplitudes.

As a first approximation, it seems reasonable to anticipate that the TMD hardening amplitudes would be bound by the bounding isothermal data. In fact, one might expect the hardening to be similar to that displayed isothermally at the average temperature of the thermomechanical cycle. This "anticipated" scenario is a fairly accurate description of what occurred at the 400 °C TMD amplitudes. The 400 °C TMD amplitudes (both in- and out-of-phase conditions) hardened slightly less than the upper bounding curve (the isothermal 427 °C data). Also, the hardening rate at this amplitude is best represented by the rate exhibited in the isothermal 427 °C test.

In contrast, the stress amplitudes incurred at the 200 °C end of the TMD cycle are not well represented by the isothermal test at 204 °C. Rather, the hardening is much greater, and actually very similar to that experienced isothermally at 427 °C. Note that the TMD hardening is greater at the 200 °C amplitude than at the 400 °C amplitude. This trend is opposite that which is suggested by the isothermal database. Similar to the 400 °C TMD amplitude, the hardening rate at the 200 °C TMD amplitude is well approximated by the 427 °C isothermal rate. The hysteresis experienced in the 200 to 400 °C tests exhibited a mild mean stress which tended to decrease with cycling, as represented by the vertical separation between the respective amplitudes.

Figure 5 shows the stress amplitude values exhibited under TMD in the 400 to 600 °C experiments. This particular condition promoted dramatic material hardening well beyond that of any other condition investigated. As seen in figure 5, the resulting behavior was not bounded by the isothermal data in terms of either stress amplitudes or total stress range, as a result of both amplitudes surpassing the greater of the isothermal conditions (593 °C).

Certain patterns observed in the 200 to 400 °C TMD tests are repeated in this temperature range. The low-temperature stress amplitudes experience greater hardening than the high-temperature stress amplitudes, again, contrary to the trends suggested by the isothermal database. Also, the TMD hardening rates are better represented by the hot-temperature bounding isothermal test, although the

400 °C TMD amplitudes eventually surpasses both the hardening rate and range of the 593 °C isothermal test.

The 600 °C TMD amplitudes are well represented by those in the bounding isothermal test at 593 °C. This applies to both the hardening rate and magnitude. However, the 400 °C TMD stress amplitudes clearly show significant deviation from the 427 °C isothermal test. Further, the hardening rates and magnitudes experienced by the 400 °C TMD amplitudes far exceed those displayed isothermally at 593 °C. This result has added significance because the 593 °C data represents the isothermal strain aging peak; thus the hardening behaviors observed in the 400 to 600 °C TMD tests exceed the entire isothermal database to the degree shown in figure 5. This unbounded behavior is clear evidence of thermomechanical path dependence, as the material's behavior at 400 °C is profoundly influenced by the previous thermomechanical history.

Shown in figure 6 are the data obtained from in-phase, out-of-phase, and bounding isothermal tests in the temperature range of 600 to 800 °C. Under this condition the isothermal data is successful at bounding the TMD material response. The 600 °C stress amplitudes of the TMD agree well with the rate and magnitude observed in the isothermal 593 °C experiment. Likewise, the hardening (or in this case softening) behavior experienced at the hot end of the TMD cycle is comparable to that observed during isothermal deformation. Although the 600 °C TMD amplitude experiences the excessive hardening associated with the isothermal strain aging peak, the total hardening range is subdued because the majority of the loading involves higher temperatures. At these slightly higher temperatures the hardening mechanisms quickly become less effective and thermal recovery processes begin to dominate. Note the large mean stress that develops in the TMD tests. This is typical of cyclic conditions which promote hardening at one end of the cycle and softening at the other.

The final TMD condition examined with a temperature range of 200 °C is that of 800 to 1000 °C and is shown in figure 7. The thermomechanical hardening trends are typified by the isothermal data, with respect to both stress magnitude and hardening rate. At these high homologous temperatures the material will tend to flow freely and offer little resistance to mechanical deformation, hence the response is essentially saturated in the first few cycles. Here thermal recovery effects dominate the behavior.

The two remaining TMD conditions are unique in the sense that they examine the effects of cycling completely through the dynamic strain aging regime. These two conditions are 300 to 800 °C and 300 to 1000 °C TMD, shown in figures 8 and 9, respectively.

The 300 to 800 °C TMD resulted in hardening trends which again show evidence of thermomechanical path dependence. The hardening behavior at the 300 °C amplitudes was similar only in rate to that experienced isothermally at 316 °C. In contrast, the hardening magnitude was found to be much greater than the isothermal 316 °C data. As shown in figure 8, the amplitudes were considerably higher than those found at the isothermal dynamic strain aging peak temperature of 593 °C. These high TMD stress amplitudes at 300 °C resulted from a continually increasing mean stress. The persistent softening occurring at the 800 °C amplitudes appears to have enhanced a stress ratchetting effect in the direction of the 300 °C amplitudes, enabling the relatively high stresses to be achieved in the fixed mechanical strain range. However, it is important to note that unlike the 400 to 600 °C TMD, the total stress range experienced is not atypical. In fact, the stress range experienced by the 300 to 800 °C TMD is comparable to that observed under isothermal conditions at 316 °C.

The TMD cycle from 300 to 1000 °C is shown in figure 9. Although the full dynamic strain aging range was spanned, it appears that the upper temperature of 1000 °C had a dominant affect on the overall deformation behavior. This condition revealed a relatively small amount of cyclic hardening at

300 °C and mild softening at 1000 °C. In contrast to the 300 to 800 °C TMD, a strong mean stress did not develop because of the inability of the 300 °C amplitude to harden.

In general, thermomechanical hardening rates appear to be dominated by effects associated with the upper-temperature of the cycle. In TMD loading cases where the isothermal data suggests that the upper-temperature condition hardens at a higher rate (200 to 400 °C and 400 to 600 °C), both TMD amplitudes hardened at the higher rate. In TMD cases where the isothermal data suggests that the upper-temperature condition is inclined to harden less (all remaining TMD conditions), the amplitudes hardened at rates similar to their isothermal counterparts, and the hardening rate of the total stress range was better reflected by the upper-temperature isothermal test. In addition, no significant differences or obvious trends were revealed between in-phase and out-of-phase hardening behaviors. A possible exception may exist at the 400 to 600 °C test condition (fig. 5) where a slight deviation at the 400 °C amplitude was observed.

Thermomechanical Microstructures

Microstructural examinations were conducted for all of the thermomechanical conditions. An attempt is made to link the microstructural features and hardening mechanisms to the observed macroscopic thermomechanical behavior. Of particular interest are the possible mechanisms leading to the "unbounded" or unique TMD behavior.

A description of the physical attributes of the TMD microstructures will be brief, as they were determined to be very similar to those developed during isothermal cycling at the maximum temperature of the TMD cycle. For example, the microstructure developed during a TMD test conducted with a temperature range of 200 to 400 °C appeared very similar to that developed during an isothermal test at 400 °C. With this knowledge, we will briefly review the thermomechanical behavior.

The microstructures developed in the TMD tests conducted from 200 to 400 °C consist of relatively high dislocation densities as a result of strong dynamic strain aging effects (but no $M_{23}C_6$). This dislocation density is considerably higher than that found isothermally at 204 °C where the dynamic strain aging effects appear to be less effectual. The TMD test develops a "400 °C microstructure" which is then subjected to loading at temperatures as low as 200 °C. Given this high dislocation density, the hardening exhibited by the 200 °C TMD amplitudes is a reasonable result. Also, since the material response at 200 °C is slightly stiffer than that at 400 °C ($E_{200\,^\circ C} > E_{400\,^\circ C}$), the magnitude of the 200 °C stress amplitude remains consistently higher than that experienced at 400 °C (fig. 4).

The microstructures developed in the 400 to 600 °C TMD tests are similar to those developed during isothermal loading at 593 °C and very similar to that which is shown in figure 3(b). This microstructure contains small precipitated $M_{23}C_6$ carbides which serve to effectively pin dislocations, and at this size clearly add to the hardening mechanisms of dynamic strain aging (solute drag). The extreme "unbounded" hardening can be at least qualitatively rationalized on the basis of this microstructure and loading temperature.

Recall that isothermal deformation below 500 °C did not promote precipitation of the $M_{23}C_6$, thus, the significant hardening (fig. 2) at 427 and 482 °C is an indication of the effectuality of solute drag without the aid of the $M_{23}C_6$ phase. The 400 to 600 °C TMD condition is unique in the sense that this small carbide is introduced into the microstructure (requiring temperatures above 500 °C) and then subjected to loads at temperatures in the vicinity of 400 °C, where the solute drag effects remain very strong and the material has greater stiffness. The result (fig. 5) is extreme hardening, as revealed by the

400 °C TMD amplitudes. This condition of "small carbides" in a microstructure loaded at 400 °C can not be represented in a strict isothermal test and as a result, the isothermal database is not capable of accurately representing the thermomechanical response.

In contrast, the 600 °C amplitudes from the 400 to 600 °C TMD tests exhibited hardening behaviors similar to that displayed isothermally at 593 °C. This is a sensible result, given that the microstructures developed in the TMD tests are indistinguishable from that which was developed in the 593 °C isothermal test.

Microstructures taken from TMD tests with upper temperatures of 800 or 1000 °C exhibit the typical overaging effects cited earlier in the high temperature isothermal tests. This was the case even for the 300 to 800 °C TMD microstructure, where the vast majority of the cyclic loading occurs at temperatures below which overaging effects occur. In the TMD conditions involving 1000 °C peaks, the microstructures were very similar to that which is shown in figure 3(d). This state clearly supports the lack of cyclic hardening experienced by the 300 to 1000 °C TMD specimen.

THERMOVISCOPLASTIC MODELING

Introduction

The TMD tests conducted in this study revealed that Hastelloy X can experience deformation behaviors which are significantly different from those exhibited under idealized isothermal conditions. This thermomechanical path dependence was found to be strongly influenced by a combination of effects associated with metallurgical instabilities and dynamic strain aging. With the aid of TEM, these phenomenological effects were qualitatively correlated with microstructural occurrences, establishing a basic understanding of the relative hardening mechanisms active under TMD conditions.

The thermomechanical behaviors of primary interest to this study are the isotropic hardening trends. It is desirable to capture two general features observed in the TMD data. First, the thermomechanical isotropic hardening must be able to exceed the baseline isothermal hardening under certain loading paths, (e.g., TMD at 400 to 600 °C). Second, thermomechanical paths involving temperatures above the strain aging peak must allow for a form of thermal recovery of the strain aging effects.

The approach taken is to extend an established macroscopic unified thermoviscoplastic constitutive theory proposed by Robinson (refs. 9 and 10). Specifically, an internal state variable and corresponding evolutionary law is formulated which attempts to track the combined effects of precipitation hardening and dynamic strain aging under full thermomechanical conditions. This extension enables the isotropic hardening rate to saturate earlier over certain thermomechanical paths. Also, certain paths will allow the hardening range and rate to exceed the baseline isothermal values. The present modeling objective is one of presenting a mathematical formulation capable of qualitatively representing the observed trends, and not one of establishing a fully characterized form for the purposes of quantitative predictions. The approach taken represents one possible methodology; other approaches to modeling deformation behavior in the presence of metallurgical changes and instabilities can be found in (refs. 17 and 18).

Mathematical Framework of the Robinson Model

The general mathematical framework used in the Robinson model evolves from a class of constitutive equations originally derived from the gradient of a complementary dissipation potential function, Ω. This function is defined as follows.

$$\Omega = \Omega(\sigma_{ij},\alpha_{ij},K,T) \tag{1}$$

$$\Omega = \Omega(F,G,T) = \theta_f(T)\int f(F)dF + \theta_g(T)\int g(G)dG \tag{2}$$

$$\text{where} \quad F = \frac{J_2}{K^2} - 1 \quad \text{and} \quad G = \frac{\hat{J}_2}{K^2}$$

$$J_2 = \frac{1}{2}\Sigma_{ij}\Sigma_{ij} \qquad \Sigma_{ij} = S_{ij} - a_{ij}$$

$$\hat{J}_2 = \frac{1}{2}a_{ij}a_{ij} \qquad a_{ij} = \alpha_{ij} - \frac{1}{3}\alpha_{kk}\delta_{ij}$$

$$S_{ij} = \sigma_{ij} - \frac{1}{3}\sigma_{kk}\delta_{ij}$$

Here σ_{ij} is the *applied* stress, α_{ij} is the *internal* (or *back*) stress, and T is the temperature. For initially isotropic materials, Ω can be taken (refs. 9, 19, and 20) to depend upon the principal invariants of deviatoric stress quantities through scalar functions F and G. The applied stress dependence enters through F which plays the role of a Bingham-Prager yield function; the *drag* stress K plays the role of a Bingham threshold shear stress (ref. 21), below which the inelastic stain rate vanishes. Models developed from this potential/normality structure have been shown (ref. 22) to be consistent with a simple thermodynamic formalism. Also, this general framework has been used (refs. 9, 10, 19, and 20) as a starting point for various viscoplastic models of isotropic and anisotropic metals.

The general framework originally introduced (refs. 9 and 10) is one which features a single evolving internal state variable. Shown below, the evolution laws for the inelastic strain, ϵ_{ij}, and *internal* stress, a_{ij}, are obtained by differentiating the dissipation potential function Ω with respect to the *applied* stress and the *internal* stress, respectively. In this form, K is taken to be a scalar constant.

$$\dot{\epsilon}_{ij} = \frac{\partial\Omega}{\partial\sigma_{ij}} = \frac{\theta_f(T)}{K^2}f(F)\Sigma_{ij} \tag{3}$$

$$\dot{a}_{ij} = -h(\alpha_{kl},T)\frac{\partial\Omega}{\partial\alpha_{ij}} = h(G)\dot{\epsilon}_{ij} - \theta_g(T)r(G)a_{ij} \tag{4}$$

$$\text{where} \qquad r(G) = h(G)g(G)$$

Equations (3) and (4) are known as the flow and evolutionary laws, respectively. Here, θ_f and θ_g are usually taken as Arrhenius type functions. The hereditary nature of the material is recorded through the

evolutionary law for a_{ij}. This second order symmetric *internal* stress tensor is a measure of the material's kinematic hardening, and physically represents an average opposing macrostress with origins in the material's dislocation microstructure.

Although many important creep/plasticity interactions can be modeled in terms of the single kinematic state variable a_{ij}, it is often necessary to incorporate features of isotropic material hardening (or softening), particularly in cases involving large numbers of cyclic loads. This is often accomplished through the evolution of the *drag* stress, K (refs. 23 and 24). The inclusion of a growth law specifying $\dot{K}$ was introduced (ref. 25) with the form shown below.

$$\text{where} \qquad \dot{K} = -H(K,T)\frac{\partial \Omega}{\partial K} + \Upsilon(T)\dot{T} = \Gamma(K,T)\dot{W} + \Upsilon(T)\dot{T} \tag{5}$$

$$\text{and} \qquad \dot{W} = \Sigma_{ij}\dot{\epsilon}_{ij}$$

This scalar internal state variable is associated with the isotropic hardening of the material, and physically represents a measure of the microstructural dislocation density. The form presented incorporates contributions to the evolution of K from effective inelastic work (W) and temperature (T). The term Υ was introduced as an extension to the evolution law obtained from the potential framework. This form allows a spontaneous change in the *drag* stress resulting from a change in temperature (i.e., a spontaneous change in the yield surface associated with a change in temperature). This feature was necessary to represent the thermomechanical path dependence observed in reference 25. Given that the main modeling interests for the present work concern the cyclic (isotropic) hardening, subsequently, emphasis will be placed on the evolution equation for the *drag* stress, K.

The function $\Upsilon(T)$ is taken as an Arrhenius form

$$\Upsilon(T) = \frac{-Q_0}{T} e^{-Q_0[T_*^{-1} - T^{-1}]} \tag{6}$$

where T_* represents a reference temperature, and Q_0 represents an "activation energy." The function $\Gamma(K,T)$ is taken as

$$\Gamma(K,T) = \Gamma_0(T)p(Z), \qquad \Gamma(T)p(0) = 0 \tag{7}$$

$$\text{where} \qquad Z(K,T) = \frac{K_s(T) - K}{K_s(T) - K_0(T)}$$

The function $K_0(T)$ is the initial value of the state variable K (before mechanical cycling) and taken as

$$K_0(T) = K^* - \left[1 - e^{-Q_0(T_*^{-1} - T^{-1})}\right]$$

$$\text{where} \qquad K^* = K_0(T_*)$$

$K_s(T)$ is the saturated value of K after extended cycling and $\Gamma_o(T)$ is a measure of the rate of hardening. Possible forms of the function $p(Z)$ are

$$p(Z) = AZ^n \quad \text{and} \quad p(Z) = A\left[1 - e^{-Z}\right]$$

By selecting appropriate forms for $K_s(T)$ and $\Gamma_0(T)$ (such as those shown in figure 10), the isothermal hardening behavior associated with dynamic strain aging is represented. Specifically, the maximum hardening (K or $\Delta\sigma$) and hardening rate $\left(\frac{dK}{dW} \text{ or } \frac{d(\Delta\sigma)}{dN}\right)$ are experienced at some intermediate "peak" temperature T_p.

Proposed Extension

The constitutive formulation discussed above was shown to be capable of qualitatively predicting several key features exhibited by Hastelloy X. These include, appropriate isothermal dynamic strain aging trends, and forms of thermomechanical path dependence exhibiting spontaneous shifts in the yield surface. However, this form is not capable of representing the isothermally "unbounded" thermomechanical trends exhibited and discussed in this study. Therefore, in an effort to represent these features, a state variable β is introduced to track the phenomenological isotropic hardening resulting from the combined effects of solute drag and $M_{23}C_6$ precipitation. The evolutionary law proposed is as follows:

$$\dot{\beta} = \Psi(T)\dot{W} - \Phi(T)$$

$$\text{where} \quad \Psi(T) = Ae^{\left[\frac{-(T-T_p)^2}{\rho}\right]} \qquad (8)$$

$$\text{and} \quad \Phi(T) = Be^{\left[Q_r(T_r^{-1}-T^{-1})\right]}$$

where T_p represents the dynamic strain aging peak temperature, Q_r and T_r are the activation energy and reference temperature for recovery effects, respectively, and A, B and ρ are material constants. The functions $\Psi(T)$ and $\Phi(T)$ are plotted in figure 11. $\Psi(T)$ is nonzero only near the peak aging temperature T_p. Thus, the first term in equation (8) is also nonzero only when the temperature is in the vicinity of T_p. Further, the first term contributes to $\dot{\beta}$ only if effective inelastic work is being incurred ($\dot{W} \neq 0$). This structure is consistent with the "dynamic" nature of the strain aging phenomenon. This framework accounts for the macroscopic hardening effects caused by the presence of the $M_{23}C_6$ carbide phase, where time spent in the vicinity of the peak temperature accompanied by inelastic work enable this phase to precipitate.

The function $\Phi(T)$ is an Arrhenius form that accounts for thermal recovery of β when the temperature exceeds the peak temperature T_p and mechanisms such as dislocation climb become significant. Time at temperature above T_p leads to $\beta < 0$ in equation (8) and allows for partial or complete erasure of hardening ($\dot{\beta} > 0$) that may have occurred by exposure to cycling at temperatures near T_p. This mathematical framework is able to simulate the observed thermal recovery and overaging effects exhibited in the microstructure of Hastelloy X, where the $M_{23}C_6$ carbides are seen to coalesce, enlarge and migrate to grain boundaries, thus "erasing" their hardening potential.

The dependence of the *drag* stress on β enters in the evolution law, equation (5), through the function Γ. Here, Γ is taken as $\Gamma(K,T,\beta)$ where dependence on β enters through the functions $K_s(<\beta>,T)$ and $\Gamma_o(<\beta>,T)$.

$$<\beta> = \begin{bmatrix} \beta; & \beta>0 \\ 0; & \beta\leq 0 \end{bmatrix}$$

This dependence is proposed as illustrated in figure 12. With $\beta = 0$, K_s and Γ_o will maintain their respective forms illustrated in figure 10. As β increases according to its evolution equation, K_s and Γ_o evolve as shown in figure 12.

As an example of thermomechanical response, assume the dynamic strain aging peak temperature (T_p) occurs at approximately 600 °C. Under thermomechanical cycling over a temperature range say, from 400 to 600 °C, the upper temperature falls precisely on T_p, the ensuing growth of β with both time and cycling allows for enhanced hardening and hardening rate at lower temperatures (e.g., 400 °C), where under isothermal cycling the hardening is, in comparison, less. Hence, this proposed form is able to qualitatively reflect the thermomechanical trends observed.

As a second example, assume the same T_p and a cyclic temperature range from 300 to 800 °C. $\Phi(T)$ will act as a competing mechanism against $\Psi(T)$, forcing β to be negative at temperatures above T_p. This, in effect, erasing some of the hardening incurred at temperatures in the vicinity of 600 °C. The resulting magnitude of β will approach zero, and the resulting thermomechanical hardening will be dominated by effects associated with the "hot" cycle temperature.

The proposed form of $\dot{\beta}$ is capable of reflecting the "unbounded" thermomechanical hardening trends observed in this set of experiments. Further, this mathematical structure allows the thermomechanical hardening to be dominated by effects associated with the "hot" end of the cycle. With this extension, the Robinson model appears suitable for representing the thermomechanical hardening trends experienced by Hastelloy X, as influenced by combined effects of dynamic strain aging and precipitation hardening.

SUMMARY AND CONCLUSIONS

Closely controlled thermomechanical deformation tests were conducted to investigate the hardening behavior of a model dynamic strain aging alloy, Hastelloy X. Isothermal and thermomechanical behaviors were compared and analyzed on the basis of phenomenological and microstructural observations. Isothermally "unbounded" thermomechanical behavior was observed over certain temperatures and qualitatively associated to physical changes on the microstructural level. With a working understanding of this association, an extension is proposed to an existing macroscopic unified thermoviscoplastic constitutive theory to give guidance and insight on modeling the thermomechanical trends. The following results and conclusions were established:

1. Dynamic strain aging effects were found to be present in Hastelloy X at temperatures ranging from ≈200 to 700 °C.

2. Precipitation of Cr-rich $M_{23}C_6$ carbides occurred at temperatures above ≈500 °C where their presence, in a nonoveraged state, promoted marked hardening.

3. Isothermal hardening trends revealed a strain aging peak at $\approx$ 500 to 650 °C with maximum increases above first cycle stress amplitudes in excess of 85 percent. This maxima was determined to be promoted by combined effects of dynamic strain aging and $M_{23}C_6$ precipitation hardening.

4. Unique thermomechanical hardening trends were found to exist under cyclic conditions where the maximum temperature did not exceed that at which microstructural overaging began ($T_{max} \leq \approx 600$ °C). Of the TMD conditions investigated, this included the 200 to 400 and 400 to 600 °C cycles.

5. Microstructures of material subjected to TMD cycles were similar to those produced during isothermal cycling at the maximum temperature of the TMD cycle.

6. An internal state variable featuring both dynamic ($\dot{W} \neq 0$) hardening and thermal recovery terms appears capable of reflecting the thermomechanical path dependent isotropic hardening in Hastelloy X.

REFERENCES

1. Baird, J.D.: Dynamic Strain Aging. The Inhomogeneity of Plastic Deformation; Papers presented at the Seminar of the American Society for Metals. ASM, Metals Park, OH, 1973. pp. 191-221.

2. Ellis, J.R., et al.: Thermomechanical Characterization of Hastelloy-X Under Uniaxial Cyclic Loading. Turbine Engine Hot Section Technology, NASA CP-2444, 1986, pp. 293-305.

3. Kotval, P.S.; and Hatwell, H., Discontinuous Precipitation of $M_{23}C_6$ Carbide in a Nickel-Base Superalloy. Trans. Metall. Soc. AIME, vol. 245, Aug. 1969, pp. 1821-1823.

4. Lewis, M.H.; and Hattersley, B.: Precipitation of $M_{23}C_6$ in Austenitic Steels. Acta Metall., vol. 13, 1965, pp. 1159-1168.

5. Tu, K.N.; and Turnbull, D.: Morphology of Cellular Precipitation of Tin from Lead-Tin Bicrystals. Acta Metall., vol. 15, 1967, pp. 369-376.

6. Singhal, L.K., and Martin, J.W.: The Growth of $M_{23}C_6$ Carbide on Grain Boundaries in an Austenitic Stainless Steel. Trans. Metall. Soc. AIME, vol. 242, May 1968, pp. 814-819.

7. Arkoosh, M.A., and Fiore, N.F.: Elevated Temperature Ductility Minimum in Hastelloy Alloy X. Metall. Trans., vol. 3, Aug. 1972, pp. 2235-2240.

8. Miner, R.V.; and Castelli, M.G.: Hardening Mechanisms in a Dynamic Strain Aging Alloy, Hastelloy X, During Isothermal and Thermomechanical Cyclic Deformation. Metall. Trans., vol. 23A, Feb. 1992, pp. 551-562.

9. Robinson, D.N.: Unified Creep-Plasticity Model for Structural Metals at High Temperature. ORNL TM-5969, 1978.

10. Robinson, D.N.; and Swindeman, R.W.: Unified Creep-Plasticity Constitutive Equations for Structural Alloys at Elevated Temperatures. ORNL TM-8444, 1982.

11. Cottrell, A.H.: A Note on the Pontevin-Le Chatelier Effect. Philos. Mag., vol. 44, no. 355, 1953, pp. 829-832.

12. Portevin, A.; and Le Chatelier, F.: Tensile Tests of Alloys Undergoing Transformation. Acad. Sci. C.R., vol. 176, Feb. 1923, pp. 507-510.

13. Tawancy, H.M.: Long-Term Characteristics of Hastelloy Alloy X. J. Mater. Sci., vol. 18, Oct. 1983, pp. 2976-2986.

14. Lai, G.Y.: An Investigation of the Thermal Stability of a Commercial Ni-Cr-Fe-Mo Alloy (Hastelloy Alloy X). Metall. Trans. A, vol. 9, June 1978, pp. 827-833.

15. Kotval, P.S.: Carbide Precipitation on Imperfections in Superalloy Matrices. Trans. Metall. Soc. AIME, vol. 242, Aug. 1968, pp. 1651-1656.

16. Castelli, M.G. and Ellis, J.R.: Improved Techniques for Thermomechanical Testing in Support of Deformation Modeling. To be published in the Proceedings of the ASTM Symposium on Thermomechanical Fatigue Behaviour, 1993.

17. Miller, A.K.: Unified Constitutive Equations for Creep and Plasticity, Elsevier, 1987, pp. 139-212.

18. Cailletaud, G.; and Chaboche, J.-L.: Macroscopic Description of the Microstructural Changes Induced by Varying Temperature—Example of IN100 Cyclic Behaviour. International Conference on Mechanical Behaviour of Materials, 3rd, K.J. Miller and R.F. Smith, eds., vol. 2, Pergamon Press, New York, 1980, Paper ONEPA TP no. 1979-112.

19. Robinson, D.N.: Constitutive Relationships for Anisotropic High-Temperature Alloys. Nucl. Eng. Des., vol. 83, 1983, pp. 389-396.

20. Robinson, D.N.; Ellis, J.R.; and Duffy, S.F.: A Viscoplastic Constitutive Theory for Metal Matrix Composites at High Temperature. Thermal Stress, Material Deformation, and Thermomechanical Fatigue; Proceedings of the 1987 Pressure Vessels and Piping Conference, ASME, New York, 1987, pp. 49-56.

21. Bingham, E.C.: Fluidity and Plasticity. McGraw-Hill, 1922.

22. Pointer, A.R.C.: General Theorems for the Dynamic Loading of Structures for a State Variable Description of Material Behaviour. Mechanical Properties at High Rates of Strain, 1979; Proceedings of the Second Conference, J. Harding, ed., Institute of Physics (Institute of Physics Conference Series, No. 47), Bristol, England, 1980, pp. 130-141.

23. Walker, K.P.: Research and Development Program for Non-Linear Structural Modeling With Advanced Time-Temperature Dependent Constitutive Relationships. NASA CR-165533, 1981.

24. Miller, A.: An Inelastic Constitutive Model for Monotonic, Cyclic, and Creep Deformation: Part I - Equations Development and Analytical Procedures. J. Eng. Mater. Technol., vol. 98, Apr. 1976, pp. 97-113.

25. Robinson, D.N.; and Bartolotta, P.A.: Viscoplastic Constitutive Relationships with Dependence on Thermomechanical History. NASA CR-174836, 1985.

TABLE I—THERMOMECHANICAL TEST MATRIX

	Temperature range, °C					
	200-400	400-600	600-800	800-1000	300-800	300-1000
In phase	1	1	1	1	1	--
Out of phase	1	1	1	1	--	1

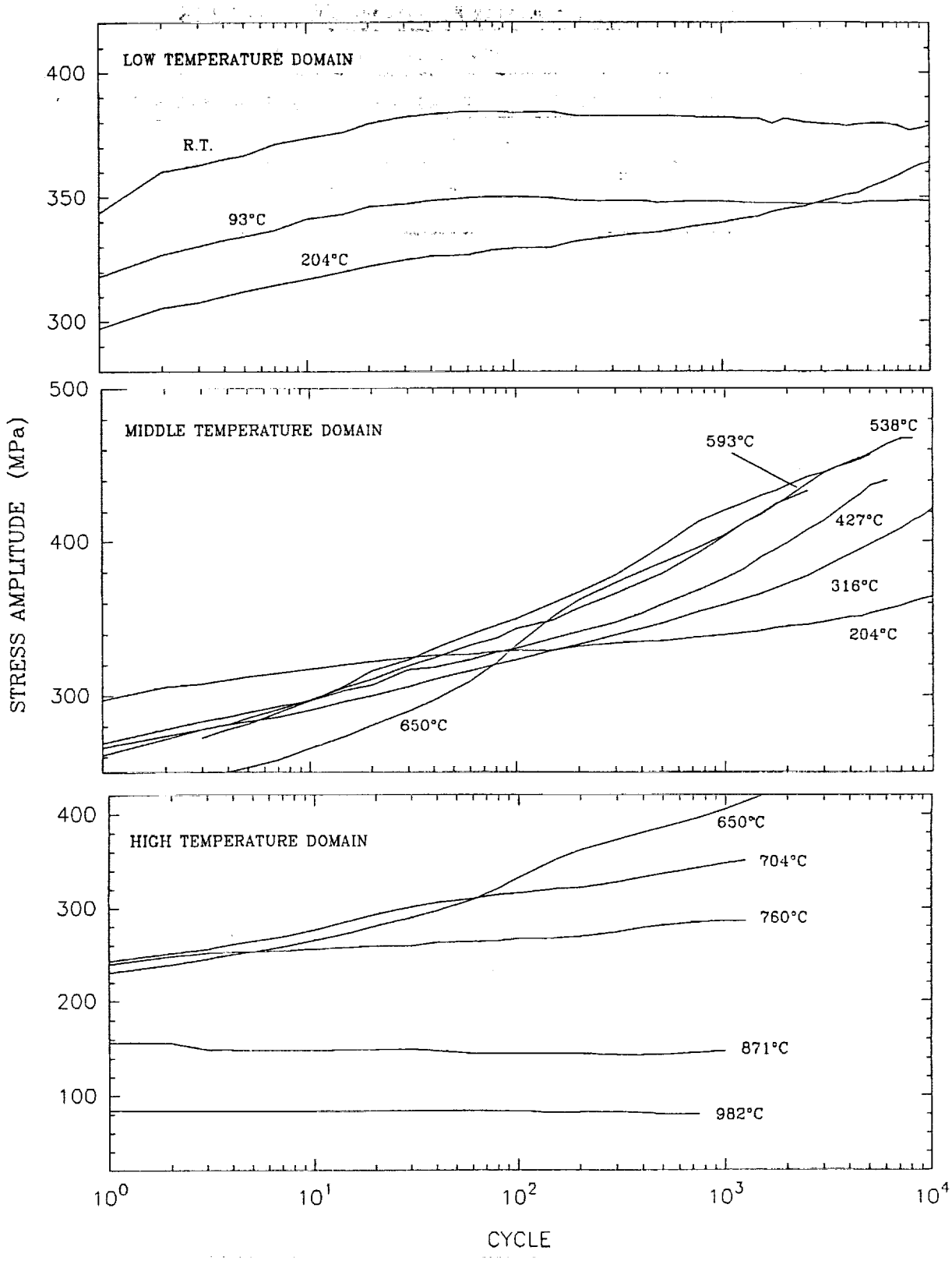

Figure 1.—Isothermal hardening behavior of Hastelloy X with $\epsilon = \pm 0.003$ and $\dot{\epsilon} = 0.001/s$ [2] over three generalized temperature domains; (a) low, (b) middle, and (c) high.

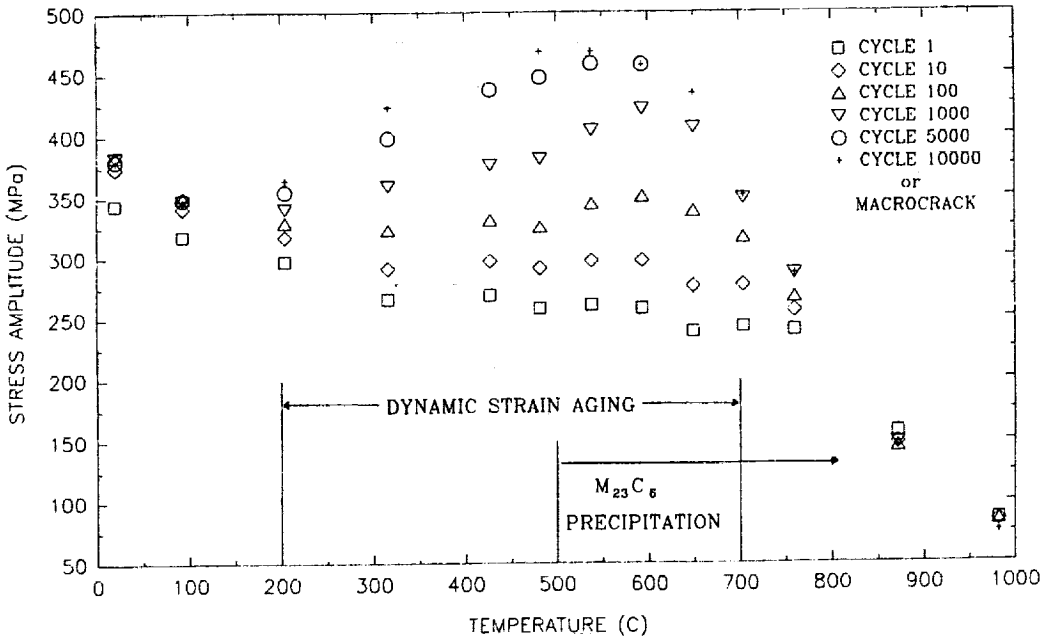

Figure 2.—Isothermal data from Fig. 1 plotted to illustrate the strain aging peak.

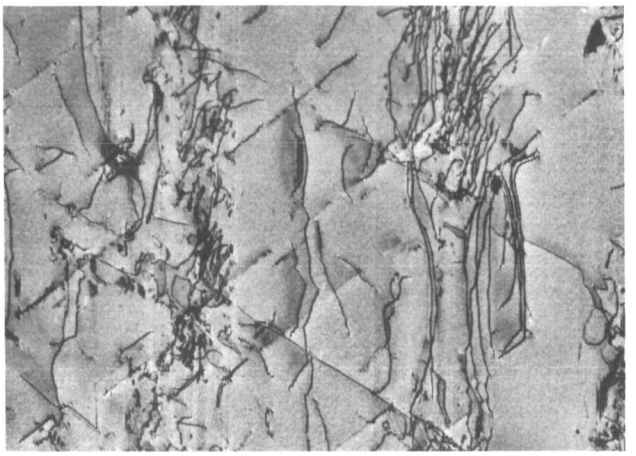

(a) 93 °C.

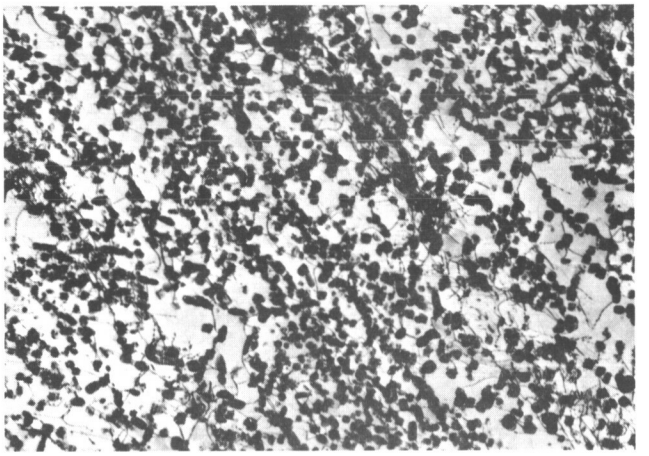

(b) 538 °C.

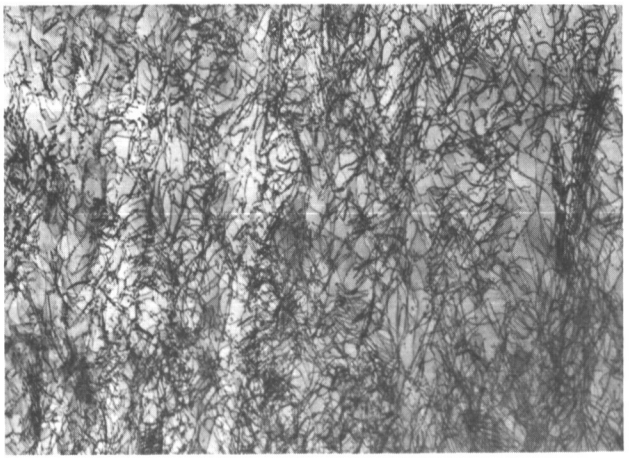

(c) 650 °C.

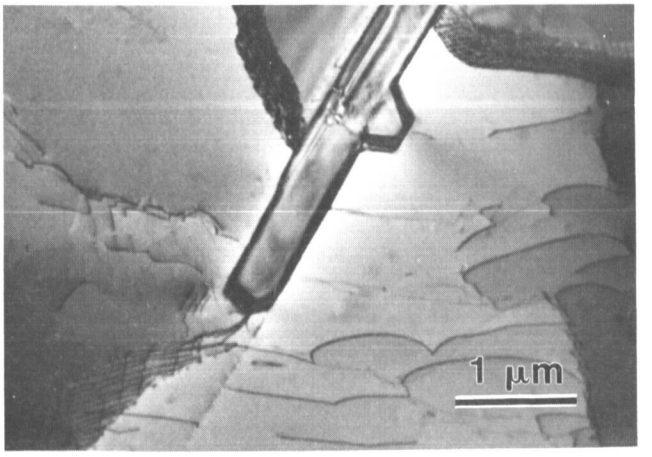

(d) 871 °C.

Figure 3.—Microstructures developed under isothermal loading conditions. See Fig. 1 for respective number of loading cycles.

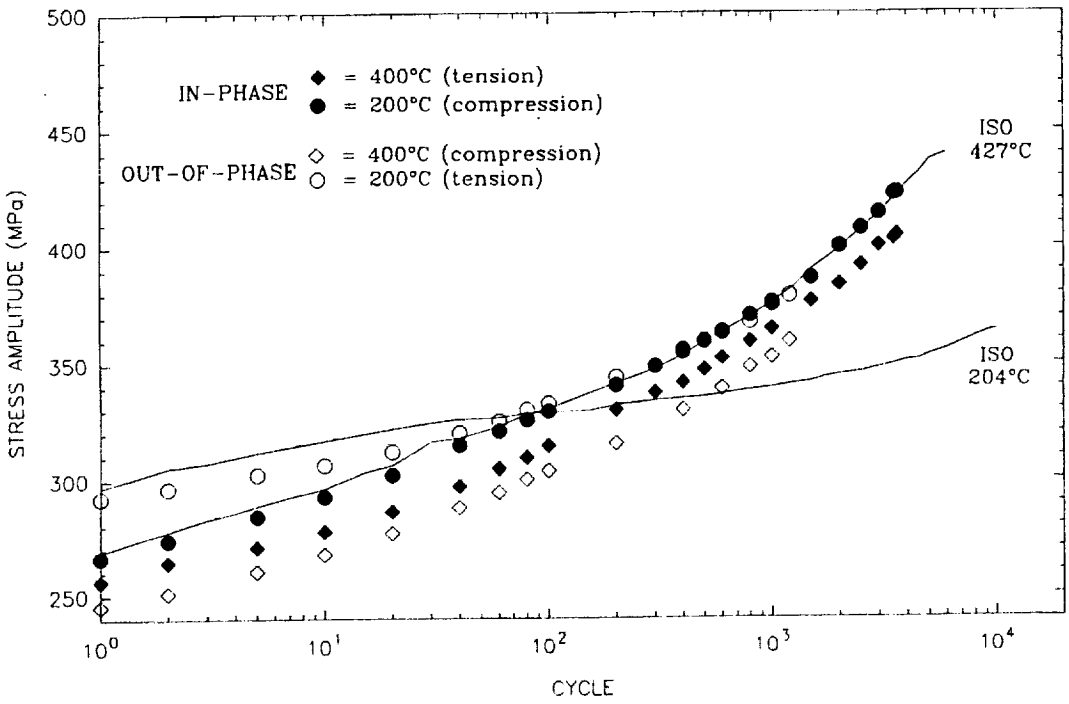

Figure 4.—Stress amplitude versus cycle plot for 200-400 °C in- and out-of-phase TMD and bounding isothermal tests.

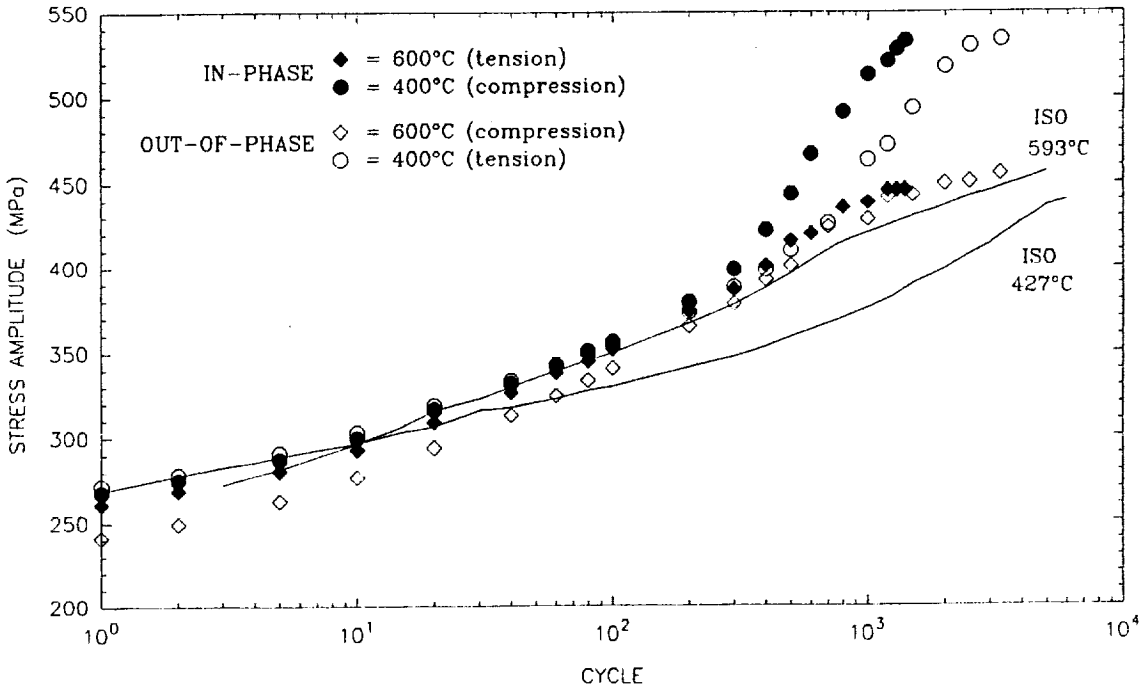

Figure 5.—Stress amplitude versus cycle plot for 400-600 °C in- and out-of-phase TMD and bounding isothermal tests.

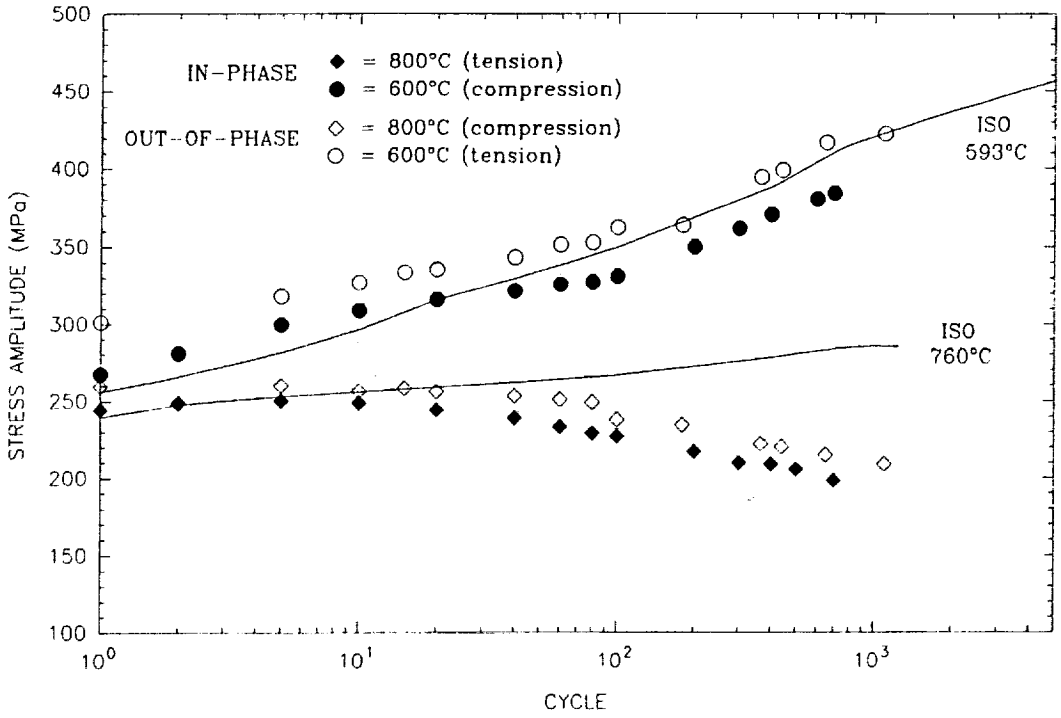

Figure 6.—Stress amplitude versus cycle plot for 600-800 °C in- and out-of-phase TMD and bounding isothermal tests.

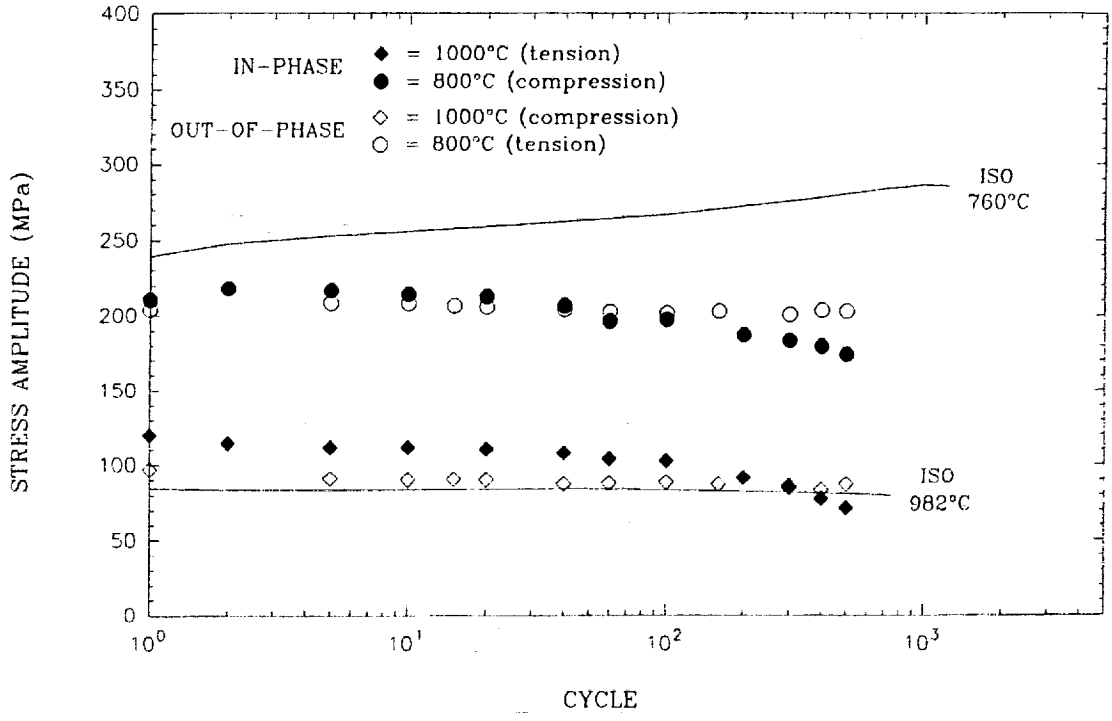

Figure 7.—Stress amplitude versus cycle plot for 800-1000 °C in- and out-of-phase TMD and bounding isothermal tests.

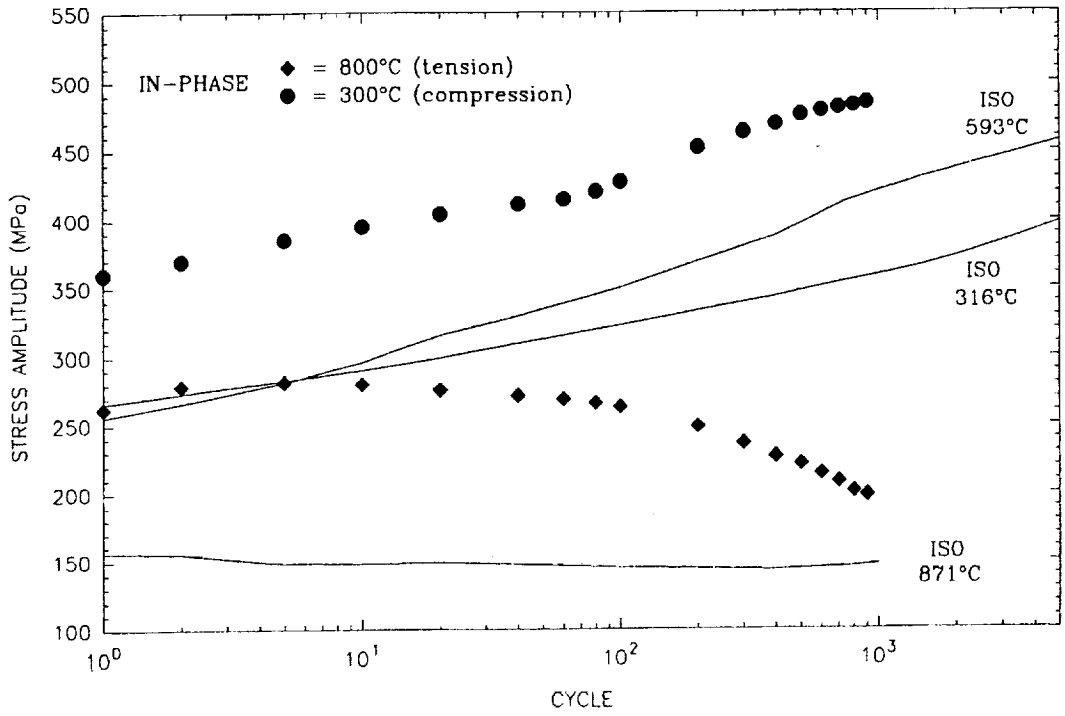

Figure 8.—Stress amplitude versus cycle plot for 300-800 °C in-phase TMD and bounding isothermal tests.

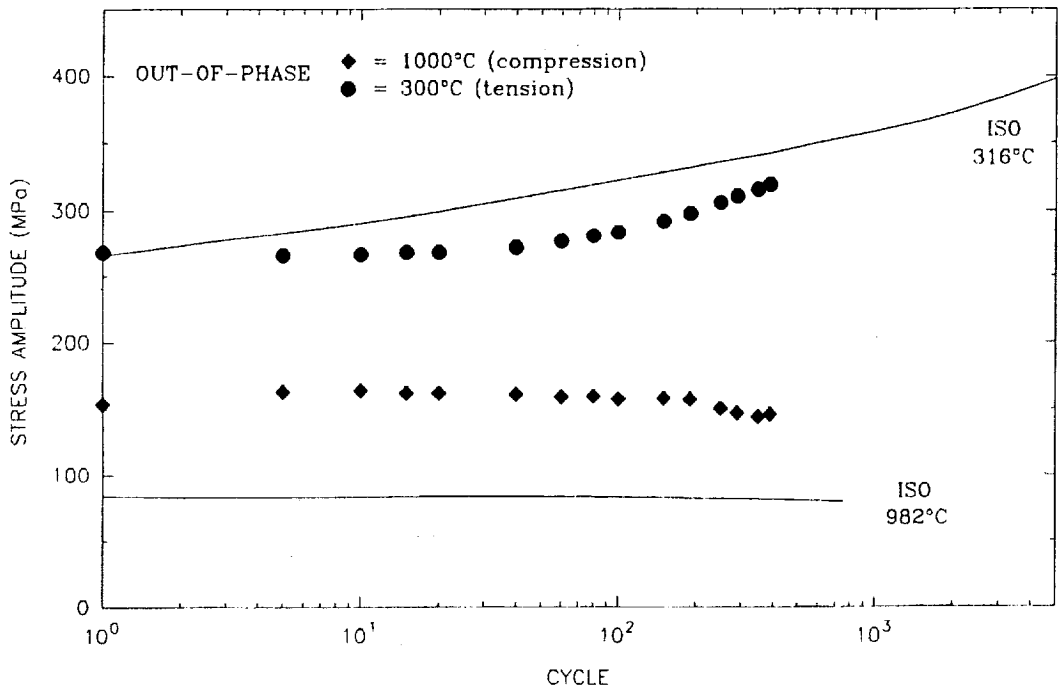

Figure 9.—Stress amplitude versus cycle plot for 300-1000 °C out-of-phase TMD and bounding isothermal tests.

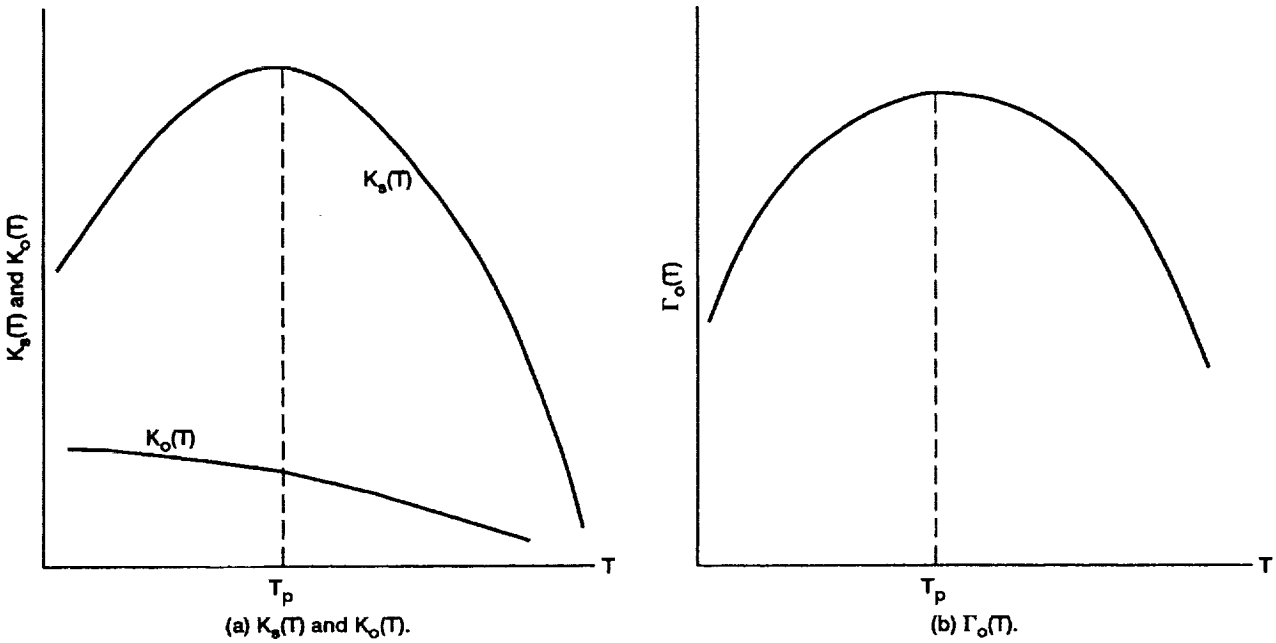

(a) $K_s(T)$ and $K_o(T)$. (b) $\Gamma_o(T)$.

Figure 10.—Appropriate forms which represent the isothermal isotropic hardening behavior associated with dynamic strain aging and precipitation hardening effects in Hastelloy X.

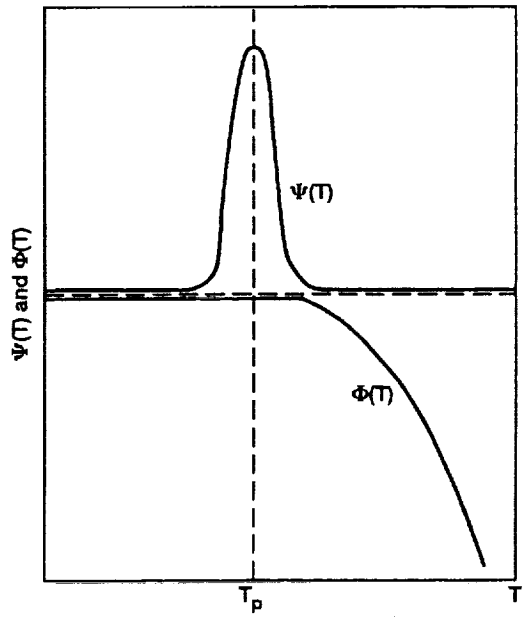

Figure 11.—Appropriate forms of $\Psi(T)$ and $\Phi(T)$ capable of representing the unbounded thermomechanical isotropic hardening features associated with dynamic strain aging and precipitation hardening in Hastelloy X.

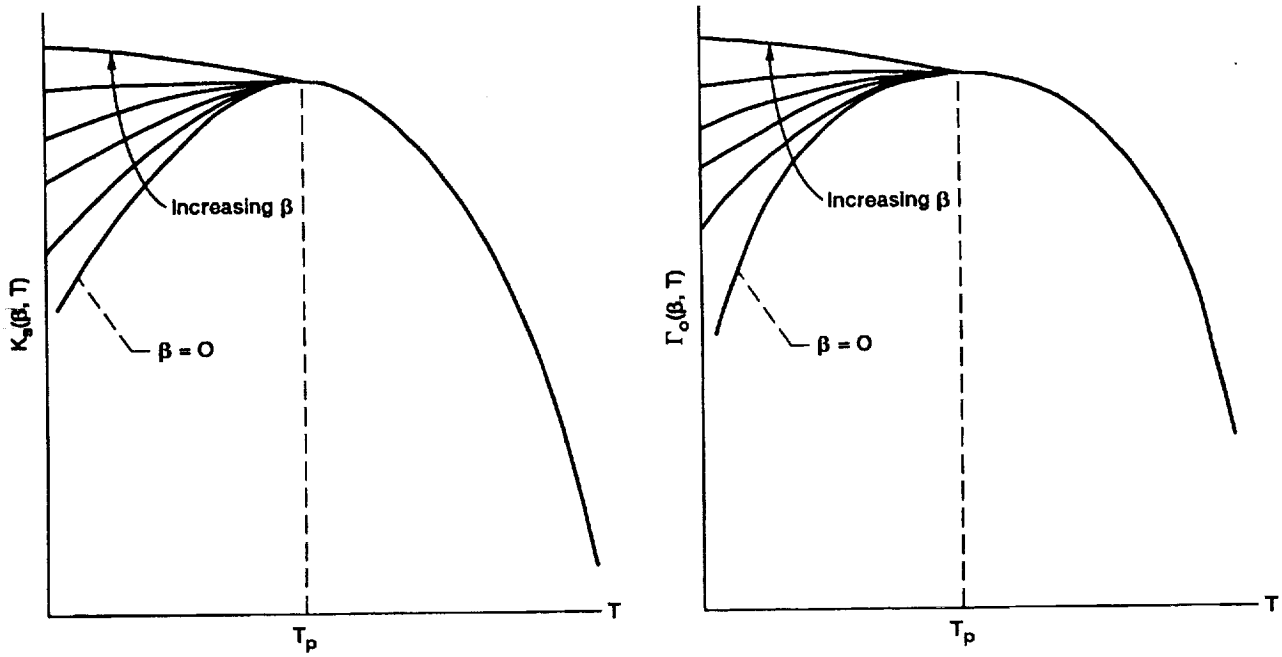

(a) $K_s(\beta, T)$.

(b) $\Gamma_o(\beta, T)$.

Figure 12.—Evolutionary trends associated with increasing β.

REPORT DOCUMENTATION PAGE

Form Approved
OMB No. 0704-0188

1. AGENCY USE ONLY (*Leave blank*)	2. REPORT DATE	3. REPORT TYPE AND DATES COVERED
	April 1992	Technical Memorandum

4. TITLE AND SUBTITLE
Thermomechanical Deformation Behavior of a Dynamic Strain Aging Alloy, Hastelloy X

5. FUNDING NUMBERS
WU-505-63-40

6. AUTHOR(S)
Michael G. Castelli, Robert V. Miner, and David N. Robinson

7. PERFORMING ORGANIZATION NAME(S) AND ADDRESS(ES)
National Aeronautics and Space Administration
Lewis Research Center
Cleveland, Ohio 44135-3191

8. PERFORMING ORGANIZATION REPORT NUMBER
E-6899

9. SPONSORING/MONITORING AGENCY NAMES(S) AND ADDRESS(ES)
National Aeronautics and Space Administration
Washington, D.C. 20546-0001

10. SPONSORING/MONITORING AGENCY REPORT NUMBER
NASA TM-105316

11. SUPPLEMENTARY NOTES
Material similar to that presented at the Symposium on Thermomechanical Fatigue Behavior of Materials sponsored by the American Society for Testing and Materials, San Deigo, California, October 16, 1991. Michael G. Castelli, Sverdrup Technology, Inc., Lewis Research Center Group, 2001 Aerospace Parkway, Brook Park, Ohio 44142 (work funded by NASA Contract NAS3-25266); Robert V. Miner, NASA Lewis Research Center; and David N. Robinson, Department of Civil Engineering, University of Akron, Akron, Ohio 44325. Responsible person, Robert V. Miner, NASA Lewis Research Center, (216) 433-3270.

12a. DISTRIBUTION/AVAILABILITY STATEMENT
Unclassified - Unlimited
Subject Category 39

12b. DISTRIBUTION CODE

13. ABSTRACT (*Maximum 200 words*)

An experimental study was performed to identify the effects of dynamic strain aging (solute drag) and metallurgical instabilities under thermomechanical loading conditions. The study involved a series of closely controlled thermomechanical deformation tests on the solid-solution-strengthened nickel-base superalloy, Hastelloy X. This alloy exhibits a strong isothermal strain aging peak at approximately 600 °C promoted by the combined effects of solute drag and precipitation hardening. Macroscopic thermomechanical hardening trends are correlated with microstructural characteristics through the use of transmission electron microscopy. These observations are also compared and contrasted with isothermal conditions. Thermomechanical behavior unique to the isothermal database is identified and discussed. The microstructural characteristics were shown to be dominated by effects associated with the highest temperature of the thermomechanical cycle. Results indicate that the deformation behavior of Hastelloy X is thermomechanically path dependent. In addition, guidance is given pertaining to deformation modeling in the context of a macroscopic unified viscoplastic constitutive theory. An internal state variable is formulated to qualitatively reflect the isotropic hardening trends identified in the TMD experiments.

14. SUBJECT TERMS	15. NUMBER OF PAGES
Thermomechanical deformation; Dynamic strain aging; Hastelloy X	26
	16. PRICE CODE: A03

17. SECURITY CLASSIFICATION OF REPORT	18. SECURITY CLASSIFICATION OF THIS PAGE	19. SECURITY CLASSIFICATION OF ABSTRACT	20. LIMITATION OF ABSTRACT
Unclassified	Unclassified	Unclassified	